

See discussions, stats, and author profiles for this publication at: <https://www.researchgate.net/publication/281121327>

Development of Control Strategies and Flight Testing of a Twin-Cyclocopter in Forward Flight

Conference Paper · May 2014

CITATIONS

13

READS

3,949

5 authors, including:



Elena Shrestha
University of Maryland, College Park

13 PUBLICATIONS 103 CITATIONS

[SEE PROFILE](#)



Vikram Hrishikeshavan
University of Maryland, College Park

52 PUBLICATIONS 489 CITATIONS

[SEE PROFILE](#)



Moble Benedict
University of Maryland, College Park

62 PUBLICATIONS 786 CITATIONS

[SEE PROFILE](#)



Derrick Yeo
University of Maryland, College Park

36 PUBLICATIONS 305 CITATIONS

[SEE PROFILE](#)

Some of the authors of this publication are also working on these related projects:



Meso-Cyclocopter [View project](#)



Quadrrotor Biplane, Package delivery drone [View project](#)

Development of Control Strategies and Flight Testing of a Twin-Cyclocopter in Forward Flight

Elena Shrestha eshresco@umd.edu Graduate Research Assistant	Vikram Hrishikeshavan vikramh@umd.edu Assistant Research Scientist	Mobile Benedict moble@umd.edu Assistant Research Scientist
Derrick Yeo dyeo@umd.edu Research Associate	Inderjit Chopra chopra@umd.edu Alfred Gessow Professor and Director	

Alfred Gessow Rotorcraft Center, Department of Aerospace Engineering,
University of Maryland, College Park, MD 20740

ABSTRACT

This paper describes the control strategies, avionics system development, and wind tunnel testing that enabled the first successful stable forward flight of a cycloidal-rotor aircraft (cyclocopter) purely using thrust vectoring. The present 550-gram vehicle has a hybrid configuration utilizing two optimized cycloidal rotors and a conventional propeller which counteracts the pitching moment generated by the cyclorotors and also provides pitch control. Stable free flight is achieved through independent rotational speed control of the three rotors and thrust vectoring of the cyclorotors through onboard closed-loop control. Since the cyclorotors spin in the same direction, there is a net angular momentum that induces a strong gyroscopic coupling between the roll and yaw degrees of freedom. The gyroscopic couplings are eliminated by implementing a careful mixing of roll and yaw inputs onboard. Unlike a conventional helicopter, a cyclocopter is propelled in forward flight purely by vectored thrust from the cyclorotors. Even though such a strategy could facilitate efficient, high-speed steady level forward flight, it is accompanied by a strong yaw-roll control cross couplings, which is in addition to the inherent gyroscopic coupling. To understand these challenges, a flight dynamics model of the vehicle derived from first principles clearly demonstrates that these couplings arise because the resultant force vector is tilted forward during forward flight. The control mixing obtained from the simulation showed good agreement with the values obtained experimentally from the wind tunnel. This mixing ratio between roll and yaw control formed the basis of the control strategy for forward flight along with aggressive closed-loop control implemented on a custom-built processor sensor board. The wind tunnel studies showed that mixing ratio was a function of phasing of blade cyclic pitch especially at high phase angles. Therefore, these mixing ratios needed to be actively changed during flight depending on phase angle. Based on these studies, steady level forward flight up to 5 m/s was successfully achieved.

NOTATION

CG	Center of gravity	L, M, N	X, Y, Z component of the moment in body reference frame
d_p	Moment arm of propeller	p, q, r	Roll, pitch, yaw rates in body reference frame
d_x, d_y, d_z	Moment arm of cyclorotor	Q_{cyclo}	Torque of cyclorotor
D_x, D_y, D_z	X, Y, Z drag components of cyclorotor	Q_{prop}	Torque of propeller
F_p	Z component force from propeller	u, v, w	X, Y, Z component of velocity vector in body reference frame
F_x, F_y, F_z	X, Y, Z lift components of cyclorotor	γ_{abs}	Absolute phase angle
H	Angular momentum of the cyclorotor	γ_{hover}	Hover phase angle
I_x, I_y, I_z	Moment of inertia in body reference frame	Φ	Phase angle with respect to hover
K	Gains used for PD controller	ϕ, θ, ψ	Roll, pitch, yaw Euler angles
k_d	Coefficient for the drag force	ω	Angular velocity of the cyclorotor

Presented at the AHS 70th Annual Forum, Montréal, Québec, Canada, May 20–22, 2014. Copyright © 2014 by the American Helicopter Society International, Inc. All rights reserved.

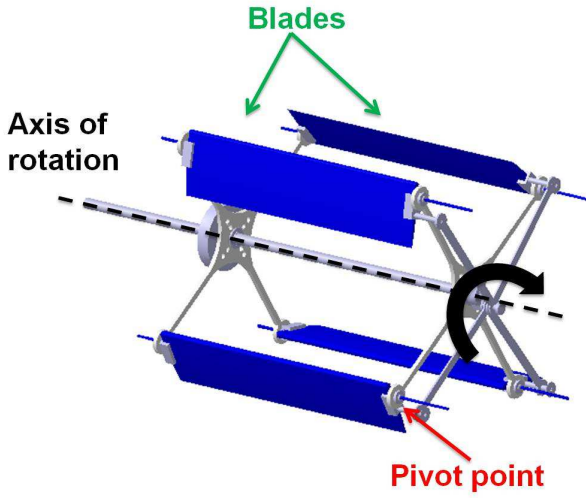


Fig. 1. Cycloidal rotor.

INTRODUCTION

Recent advancements in microelectronics has led to the emergence of a scaled-down class of Unmanned Aerial Vehicles (UAVs) known as Micro Air Vehicles (MAVs). As a highly portable versatile flying platform, MAVs have widespread application in both military and civilian settings for missions ranging from reconnaissance, search-and-rescue, border surveillance, to traffic monitoring. These types of missions require high endurance, maneuverability, and hover/low-speed flight capability. To serve these missions, different configurations of rotary-winged MAVs have been developed including conventional single main rotor/tail rotor, co-axial rotor, and quad-rotor designs. While successful at larger scales, conventional edgewise rotors have degraded performance at low Reynolds number (10,000 – 50,000), which is the operating range for MAVs. While efficient full-scale conventional rotors achieve a figure of merit (FM) up to 0.82, an optimized conventional MAV rotor can only achieve approximately 0.65 in comparison (Refs. 1,2).

In the past, hover-capable biomimetic flapping-wing platforms have been proposed as an alternative to conventional rotary configuration. These flapping-wing concepts offer higher maneuverability and gust tolerance, but typically have greater mechanical complexities because of the need to produce high frequency flapping motions. In addition, much of the tools needed to understand the unsteady aerodynamics encountered by flapping wings are still in early stages of development, restricting the flapping-wing platforms from successfully competing with existing rotary-wing concepts.

Another fundamentally efficient alternative is the cyclocopter, a revolutionary cycloidal rotor-based MAV. The blades on the cycloidal rotor (cyclorotor) follow a circular trajectory about a horizontal axis of rotation (Fig. 1). The cyclorotor blade span is parallel to the horizontal axis and perpendicular to the direction of flight. A pitching mechanism cyclically varies individual blade pitch angle along a circular trajectory. In hover, the blades achieve a positive geometric pitch angle

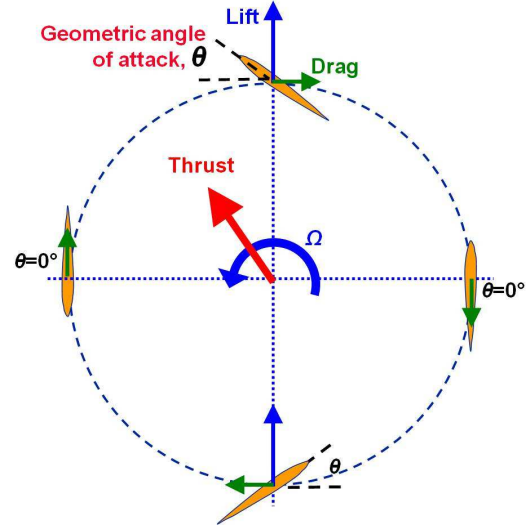


Fig. 2. Blade kinematics.

at both top and bottom portions of the trajectory, yielding a net resultant thrust (Fig. 2). Both the magnitude and direction of the thrust vector can be adjusted by varying the pitch amplitude and phasing of the blade pitching kinematics.

When compared to a conventional edgewise rotor at the same disk loading (thrust/disk area), an optimized cyclorotor has a higher power loading (thrust/power) in hover (Fig. 3). Since all spanwise blade sections of the cyclorotor operate under similar aerodynamic conditions (i.e., flow velocity, angle of incidence, Reynolds number, etc.), the blades can be easily optimized to achieve best aerodynamic efficiency. In addition, the uniform spanwise distribution of aerodynamic forces enables the cyclorotor to operate at lower tip speeds, thereby improving the acoustics signature. Another advantage of the cyclorotor is its unique thrust vectoring capability that is achieved by varying the phase of the cyclic pitching. By thrust vectoring instead of pitching forward, the cyclocopter can achieve level forward flight in a power efficient manner. This will be discussed in more detail in the following sections. Thrust vectoring also improves maneuverability and promotes the vehicle's operation in gusty environments.

Previous work performed at the University of Maryland has led to the development of many cyclocopter configurations (ranging from 130 to 800 grams) capable of stable and autonomous hover (Refs. 3–5). To evaluate the vehicle's tolerance to external wind-gust disturbances, a comprehensive flight dynamics model in hover was developed experimentally using a time domain system identification technique (Ref. 6). The study determined the existence of a destabilizing gyroscopic coupling between roll and yaw degrees of freedom, which required implementation of decoupling methods in the controls system. When compared to other rotary-based MAV platforms, the cyclocopter had higher longitudinal and lateral gust tolerances. The flight dynamics model derived from the study revealed many key insights into the vehicle's maneuverability in hover conditions and led to an improvement of the controls system.

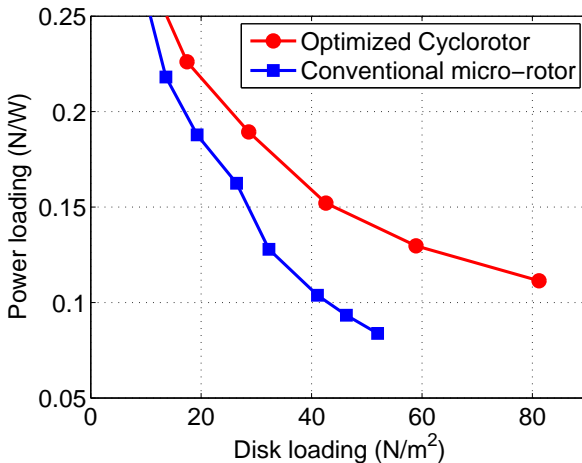


Fig. 3. Power loading (thrust/power) vs. disk loading (conventional micro-rotors vs. optimized cyclorotor)

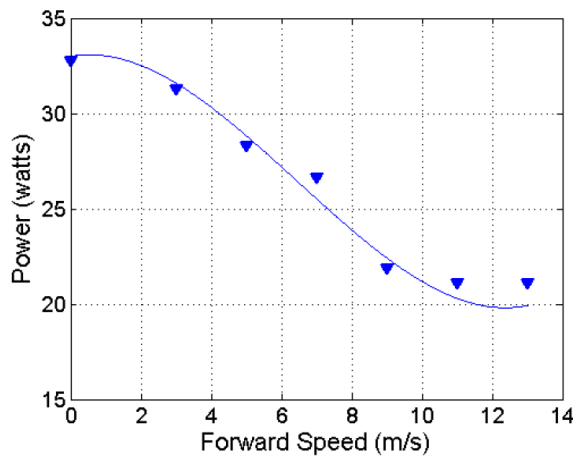


Fig. 4. Power versus forward speed for constant rotational speed of 1740 rpm (13.88 m/s) for level, steady flight.

Recently, wind tunnel studies on an isolated cyclorotor have shown that an aircraft using cyclorotors could efficiently reach very high forward speeds without any lift augmenting devices/surfaces (Refs. 7–9). It was observed that the power required for a cyclorotor to maintain a steady, level flight significantly drops with forward speed (Fig. 4) up to almost an advance ratio of 1, due to increased lift producing efficiency of the cyclorotors. Unlike a conventional helicopter, the forward flight of a cyclocopter would be performed purely by utilizing thrust vectoring (varying cyclic pitch phasing) instead of pitching the entire vehicle forward. Thrust vectoring enables the cyclocopter to maintain a level pitch attitude in forward flight. Unlike the transition for a tilt-rotor, transition from hover to forward flight for the cyclocopter is possible without undergoing any configuration changes. Overall, thrust vectoring provides a mechanically simple and power efficient method of achieving forward flight.

The present work aims to develop a forward flight control strategy for the twin-cyclocopter by using a combination of independent pitch phasing and rotational speed control of the

two cyclorotors and the propeller. A flight dynamics model in forward flight was formulated using a first principles approach in order to develop strategies to decouple the roll and yaw dynamics in forward flight. The paper initially discusses the methodology used to construct the linearized dynamics model. Results from the simulation were used to develop a control strategy to achieve decoupled forward flight. This was tested in a partially constrained (5-DOF) wind tunnel setup at various forward velocities. Finally, free flight test results are presented. Attitude and airspeed data recorded by the onboard processor show that the vehicle successfully achieves steady, level forward flight.

CYCLOCOPTER VEHICLE SPECIFICATION

A 550 gram twin-rotor cyclocopter was developed with a hybrid configuration utilizing both the cyclorotor and a conventional rotor. Since both the cyclorotors spin in the same direction, a large pitching reaction moment needed to be counterbalanced by the forward-mounted propeller. The vehicle has a lateral dimension of 0.381 meters (1.25 feet), longitudinal dimension of 0.457 meters (1.5 feet), and a height of 0.305 meters (1 foot) (Fig. 5). Each cyclorotor has a diameter of 0.152 meters (6 inches), blade span of 0.171 meters (6.75 inches), a chord of 0.051 meters (2 inches), and is independently driven by a 75 watts out-runner motor through a 7.5:1 single-stage transmission. The horizontal nose rotor is directly driven by a 920kV brushless outrunner motor and is fitted with a 3-bladed GWS 9050 propeller. All three rotors are powered by a single 3S 11.1 volt 850 mAh Lithium-Polymer battery. A detailed weight distribution of all the components is provided in Table 1.

The parameters (blade pitching amplitude, location of pitch axis, rotor radius, blade airfoil, chord, planform, etc.) of the present cyclorotor have been optimized through series of systematic experimental studies conducted in the past (Refs. 10–14). Each blade uses a NACA 0015 airfoil, a symmetric pitching amplitude of 45°, and a chord/radius of 0.625. All of the design parameters of the cyclorotor are summarized in Table 2. Leveraging the insights gained from these studies, the present cyclorotor is designed for maximum thrust-to-power ratio (power loading) in hover and maximum power efficiency in forward flight. While optimizing the rotor parameters for maximum aerodynamic performance, emphasis was also placed on the blade and rotor structural design to reduce the overall rotor weight (Refs. 3–5).

Blade Pitching and Thrust Vectoring Mechanism

The schematic of the blade pitching mechanism is depicted in Fig. 6 where the four bars of the linkage system are labeled L_1 , L_2 , L_3 and L_4 . L_1 , also referred to as rotor radius, is the distance between the blade pitching axis and the horizontal axis of rotation. The pitch links (of length L_3) are connected to the end of the offset link on one end and the other end is connected to point B which is at a distance L_4 behind the pitching axis. The connections at both ends of the pitch link are

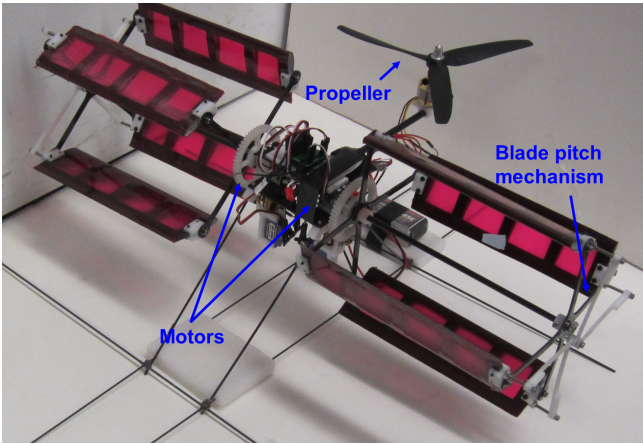


Fig. 5. 550 gram twin-cyclocopter.

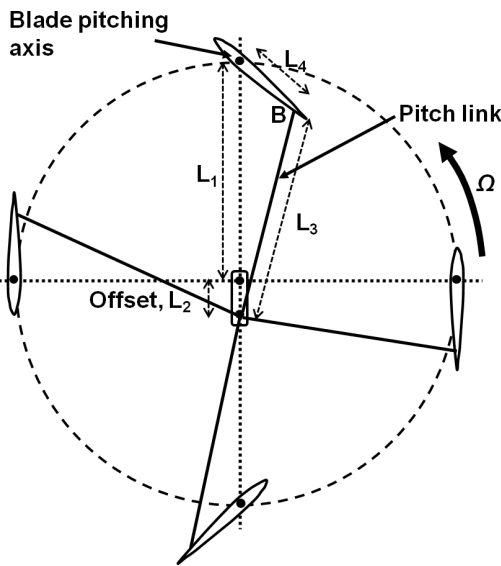


Fig. 6. Four-bar linkage based pitching mechanism.

through pin joints to allow the rotational degree of freedom. With this arrangement, as the rotor rotates, the blades automatically pitches cyclically, where the pitching amplitude depends on the offset length, L_2 , when the other linkage lengths remains fixed. The rotation of the offset link changes the phasing of the cyclic pitching and thereby changes the direction of the thrust vector.

The actual pitching mechanism implemented in the vehicle

Table 1. Weight distribution of the 550 grams twin-cyclocopter.

System	Weight (g)	% Total
Cyclorotors	155	28.1
Electronics	30	5.5
Propeller System	70	12.7
Battery	90	16.4
Structure	130	23.7
Actuators	75	13.6
Total	550	100%

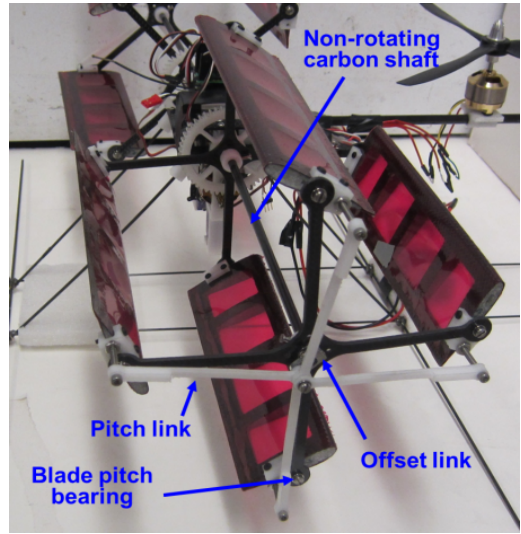


Fig. 7. Pitching mechanism on the cyclorotor.

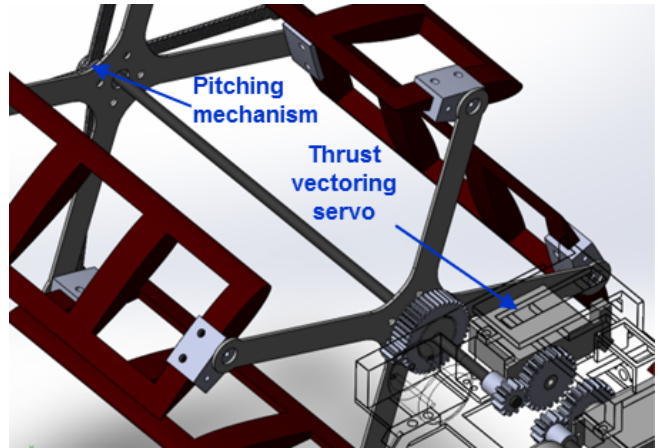


Fig. 8. Thrust vectoring mechanism.

cle is shown in Fig. 7. For the present pitching mechanism to work, the offset link (L_2) needs to be installed at the tip of shaft in a non-rotating frame. In order to reduce mechanical complexities, the distance L_2 is kept constant, hence the blade pitching amplitude could not be actively varied in flight. Therefore, the only way to alter the magnitude of the thrust is to vary the rotational speed of the rotors. As mentioned, the direction of the thrust vector can be manipulated by rotating the offset link.

For the current setup, thrust vectoring is actuated using two

Table 2. Design parameters of the cyclorotor.

Parameter	Cyclorotor
Rotor Diameter	0.152 meters (6 inches)
Blade span	0.171 meters (6.75 inches)
Blade chord	0.051 meters (2 inches)
Blade airfoil	NACA 0015
Blade pitch amplitude	$\pm 45^\circ$
Blade pitch axis	45% from LE

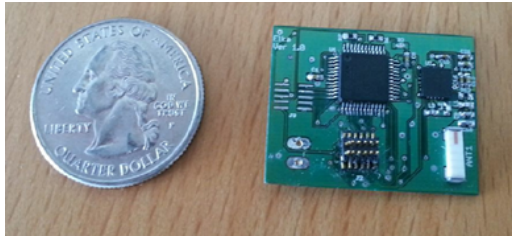


Fig. 9. ELKA, 1.3 gram processor-sensor board developed at UMD.

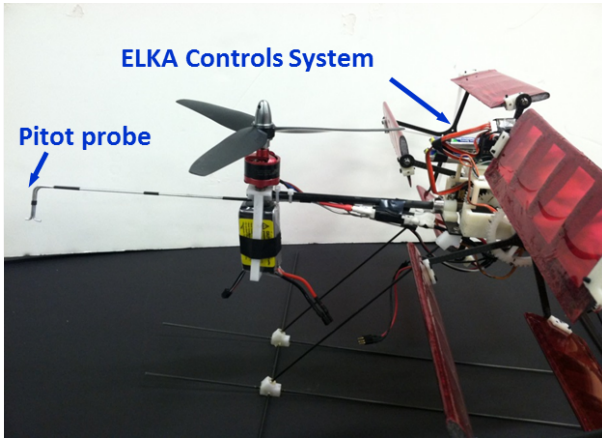


Fig. 10. Airspeed sensor package.

servos that are connected to the pitching mechanism through a 2:1 transmission (Fig. 8). Using this gear arrangement, the offset link is rotated and the pitch phasing could be changed up to 120° .

ONBOARD INSTRUMENTATION

Without additional attitude stabilization through a closed-loop feedback system, the cyclocopter was found to be highly unstable due to the presence of strong gyroscopic roll-yaw coupling and limited inherent aerodynamic damping (Ref. 6). Attitude stabilization is implemented onboard using ELKA, a custom embedded processor-sensor board developed for the twin-cyclocopter (Fig. 9). The board weighs only 1.3 grams and is powered by a single 1-cell 3.7 volt 125mAh Li-Po battery. ELKA houses a STM32 microprocessor with a 32-bit ARM Cortex M3 core for high-end onboard computation tasks. The MPU-9150 IMU integrated on the board includes tri-axial gyroscopes, accelerometers, and magnetometers. Wireless communications are serviced by an on-board nRF24L01 chip, a low-power 2.4 GHz RF transceiver. ELKA has a sensor update rate of 500 Hz and is capable of streaming vehicle attitude data and actuator controls data to the base station with a short latency.

Due to the unique requirements of a small cyclocopter, a novel air data system was required to successfully record airspeed data in forward flight (Fig. 10). A custom forward-mounted airspeed probe was designed and fabricated using

techniques developed in previous work (Ref. 15). By using a pair of fore-aft facing pressure ports, low translational air velocities can be measured using a scaled version of the pitot static equations. These ports are connected to the differential pressure inputs on a high sensitivity Honeywell HSCDRR series pressure sensor. A second ARM Cortex M4 microprocessor dedicated to air data measurements is used to take 13-bit measurements at 250 Hz. To account for the complex local flow-field generated by the cyclorotors, a second airspeed calibration was carried out in the wind tunnel with the probe mounted and with the rotors spinning to simulate the flow conditions encountered in forward flight.

Telemetry

The user communicates with the onboard controller using a LabVIEW interface through a wireless IEEE 802.15.4 data link (Fig. 11). The board receives pilot inputs through a commercial Spectrum receiver which connects to the transmitter through a wireless 2.4 GHz radio link. A separate connection between the Spectrum receiver and transmitter ensures that the pilot will still have command over the vehicle if connection is lost between the ground station and the onboard processor. The ground station allows the user to modify the gains of the feedback system, change sensitivity of pilot inputs, and record attitude data transmitted by the onboard processor. All the data processing, feedback control calculations, and roll-yaw decoupling methods are performed by ELKA.

CLOSED-LOOP FEEDBACK CONTROL

Onboard closed-loop feedback is implemented using a proportional-derivative (PD) controller as shown in (Fig. 12). The PD controller on the vehicle has been proven sufficient at the operating forward velocities and small aerodynamic disturbances (indoor flight).

The feedback states are aircraft pitch and roll Euler angles (ϕ, θ) and the attitude rates (p, q and r). An outer loop for translational positioning is performed by a remote pilot. The final control inputs to the vehicle actuators are the individual rotational speeds of the rotors and the two servo inputs.

The pitch (q), roll (p), and yaw (r) attitude rates are extracted from the tri-axial gyroscopes and combined with the data provided by the accelerometer to produce precise attitude measurements. The integration of gyro measurements with time has been known to cause drift in attitude estimation (Refs. 16, 17). To account for the drift, a high pass complementary filter is used with a 4 Hz cut-off frequency for the gyro measurements. Vibrations from the rotary systems affected accelerometer measurements, which are processed through a low pass complementary filter with a 6 Hz cut-off to reject disturbances from the rotor vibrations occurring at significantly higher frequencies than the body dynamics.

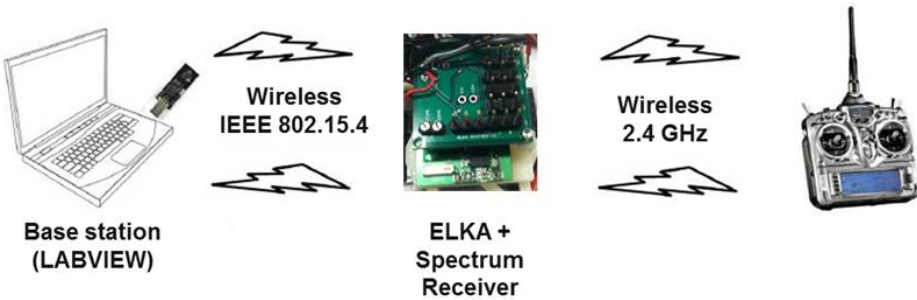


Fig. 11. Telemetry.

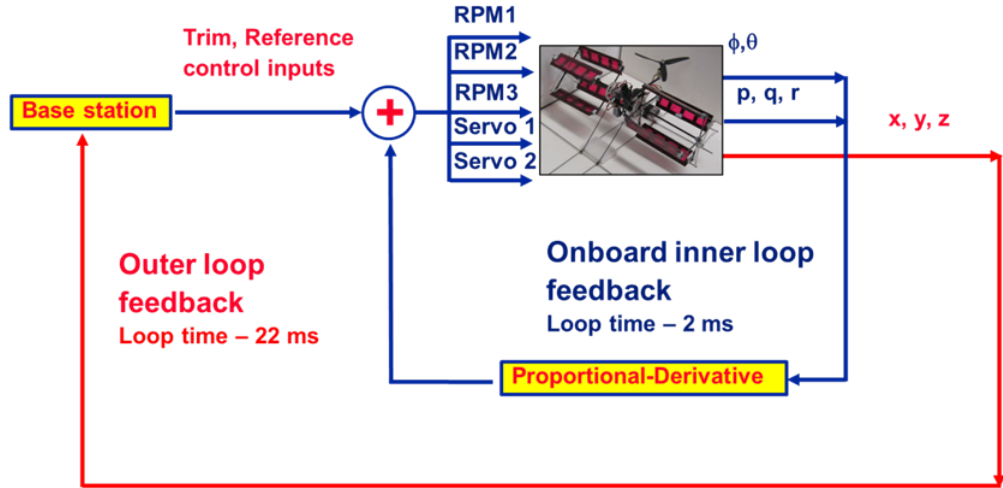


Fig. 12. Closed-loop feedback system.

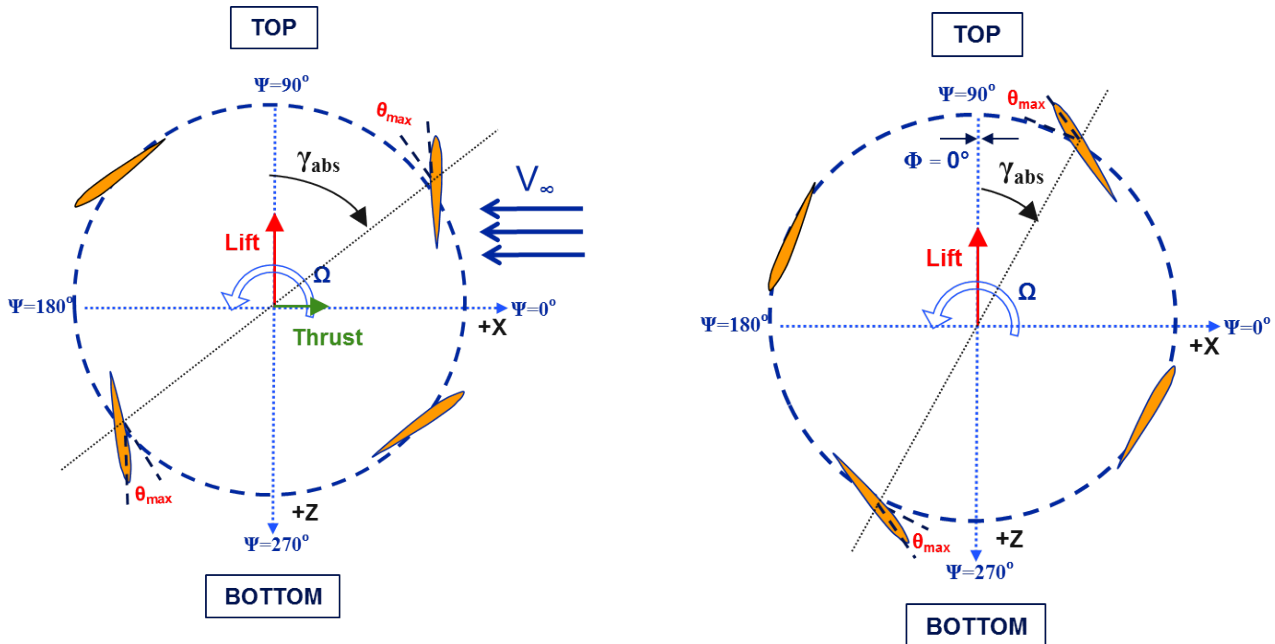


Fig. 13. Cyclorotor coordinates showing measurement of absolute phase angle (γ_{abs}), lift force, and propulsive force in forward flight.

Fig. 14. Schematic showing hover condition with $\gamma_{abs} > 0^\circ$ and $\Phi=0^\circ$.

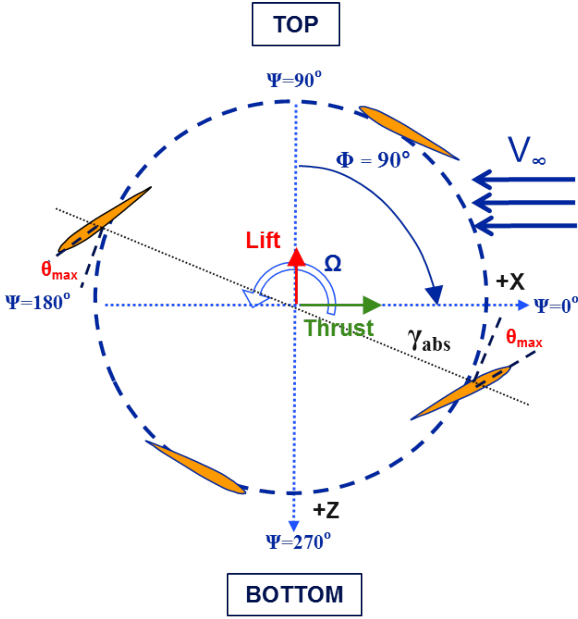


Fig. 15. Cyclorotor coordinates at maximum forward flight where $\gamma_{abs} > 90^\circ$ and $\Phi=90^\circ$.

CYCLOROTOR KINEMATICS IN FORWARD FLIGHT

The coordinate system used for the cyclorotor is shown in (Fig. 13). The time-varying aerodynamic forces produced by the cyclorotor can be resolved into the vertical and horizontal directions. The azimuthal position of the blade (Ψ) is measured counter-clockwise from the horizontal axis of rotation and is equivalent to zero when the blades are rightmost side of the circular trajectory. The blade pitch angle (θ) is the angle between the blade chord and the line tangent to blade path. The absolute phase angle (γ_{abs}) is defined as the relative azimuthal location of the maximum blade pitch angle with respect to the $-Z$ -axis. When $\gamma_{abs} = 0^\circ$, the maximum blade pitch occurs at the top of the circular trajectory and when $\gamma_{abs} = +90^\circ$, the maximum occurs $+90^\circ$ clockwise towards the direction of flow.

The lift and propulsive force components are defined as the net aerodynamic forces produced along the $-Z$ -axis and $+X$ -axis. For the present cyclorotor, the pitch amplitude is kept constant and the magnitude of the net resultant thrust vector is controlled by varying the cyclorotor rotational speed. The direction of the thrust vector is rotated through cyclic pitch phasing. To achieve a stable hover, the phase angle must be rotated such that the resultant thrust vector is purely vertical. For the remainder of the paper, the forward flight phase angle (Φ) of the cyclorotor, distinct from the absolute phase angle of each blade, is defined with respect to the phase in hover (γ_{hover}).

$$\Phi = \gamma_{abs} - \gamma_{hover} \quad (1)$$

A forward flight phase angle of $\Phi = 0^\circ$ corresponds to the hover condition when there is a net lift component and zero propulsive force (Fig. 14). As shown in (Fig. 15), the phase

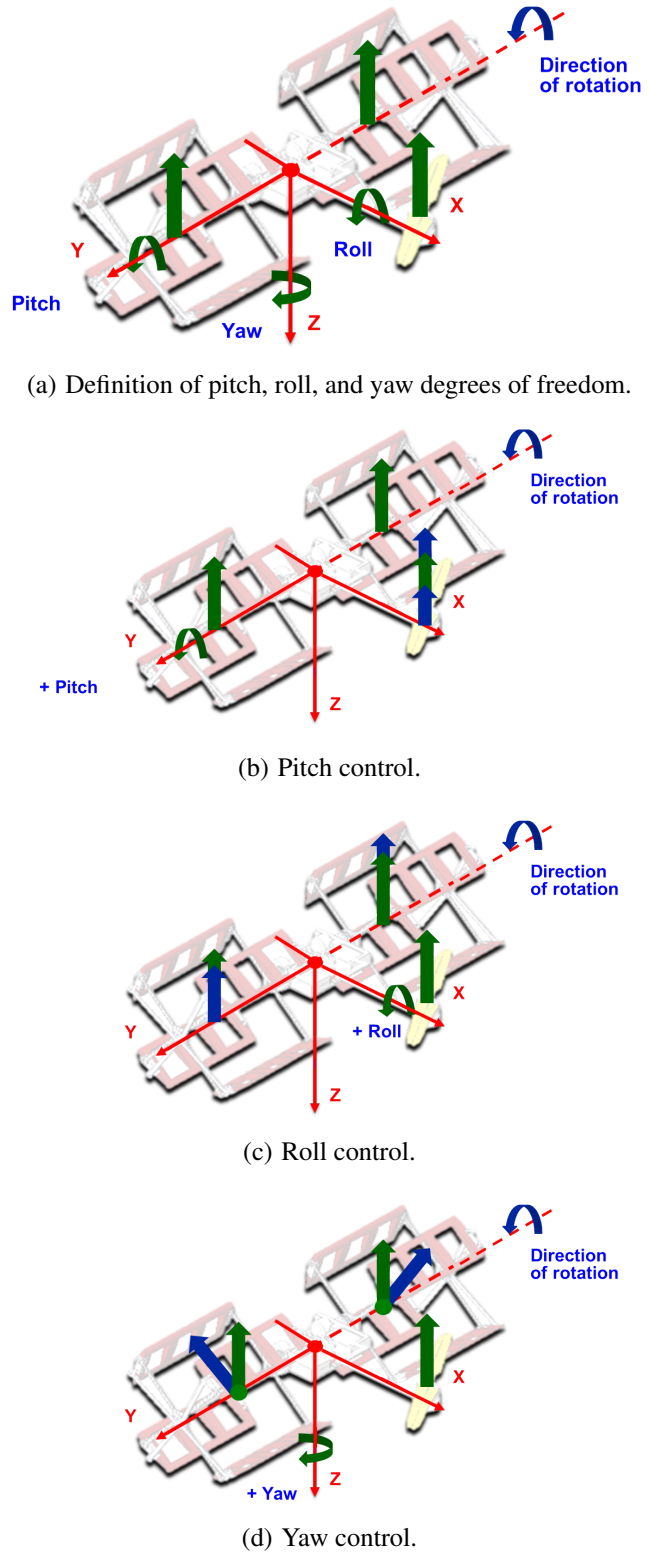
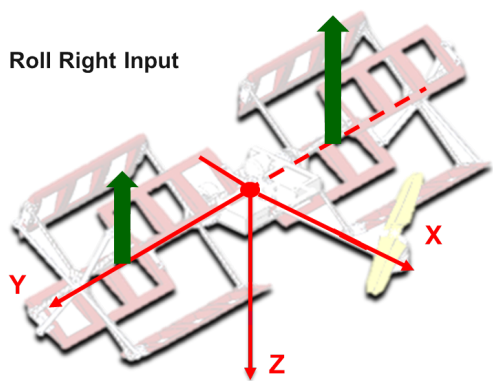
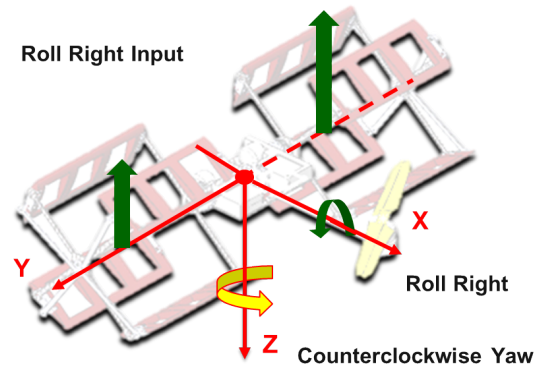


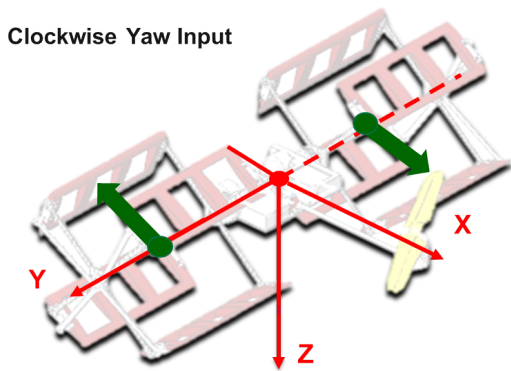
Fig. 16. Control strategy for twin-cyclocopter.



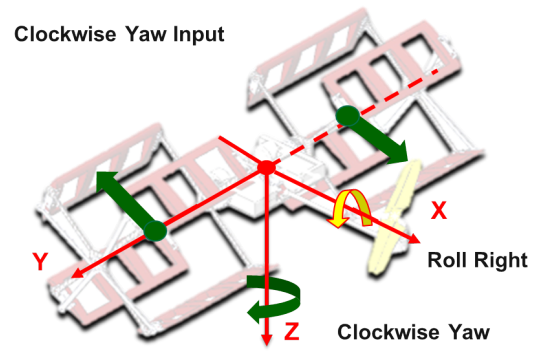
(a) Roll right control input.



(b) Roll-yaw response.



(c) Yaw control input.



(d) Yaw-roll response.

Fig. 17. Gyroscopic cross-coupling between roll and yaw degrees of freedom.

angle for maximum propulsive force in forward flight is limited to $\Phi = +90^\circ$.

The phasing of cyclic blade pitch plays a significant role in trimming the cyclorotor in forward flight and this will be discussed in further detail in the next section.

Attitude Control in Hover

Fig. 25(a) shows the definition of pitch, roll, and yaw degrees of freedom for the twin-cyclorotor. As previously mentioned, both the cyclorotors rotate clockwise in the same direction such that there is a pitch-down moment that must be counteracted by a horizontal nose rotor (Fig. 25(b)). Stable hover, transition, and forward flight require a unique combination of independent rotational speed of all three motors and thrust vectoring of the cyclorotors for each mode of flight.

A positive roll is produced by increasing the rpm of the left rotor and decreasing the rpm of the right rotor (Fig. 25(c)). Finally, yaw is controlled through differential rotation of the two cyclorotor thrust vectors (Fig. 25(d)). The cyclorotors spin in the same direction along the +Y-axis so there is a net angular momentum that induces gyroscopic coupling between the roll and yaw degrees of freedom. To eliminate the gyroscopic coupling, an onboard control mixing was implemented where the roll and yaw inputs were appropriately combined to give decoupled motion.

Attitude Control in Forward Flight

In forward flight, the combined forward flight phase actuation of cyclic blade pitch is utilized to control the forward velocity of the vehicle. Providing a cyclic pitch phasing for both cyclorotors rotates the resultant thrust vectors by the same phase angle. Essentially, an increase of the combined forward flight phase angle would result in a higher propulsive force contribution from the cyclorotors. As in hover, pitch, roll, and yaw moments in forward flight are controlled through propeller rpm, differential cyclorotor rpm, and differential thrust vectoring, respectively. The pilot controls now include throttle (collective cyclorotor rpm), pitch (propeller rpm), roll (differential cyclorotor rpm), yaw (differential phasing), and forward velocity (collective phasing).

For the cyclorotor, transitioning from hover to forward flight does not involve any configuration changes. By slowly increasing the phase angle, the vehicle is able to steadily increase forward velocity and transition into forward flight. The rate of transition from hover to forward flight depends entirely on the phasing input. When transitioning back to hover, the cyclorotor is able to abruptly come to a stop even while moving at reasonable forward velocities. The phasing of pitch provides complete control authority of the forward velocity.

One of the major challenges in developing the forward flight control strategy is the existence of a strong coupling between the roll and yaw control that increase with the forward tilt of the thrust vector. Furthermore, this coupling is

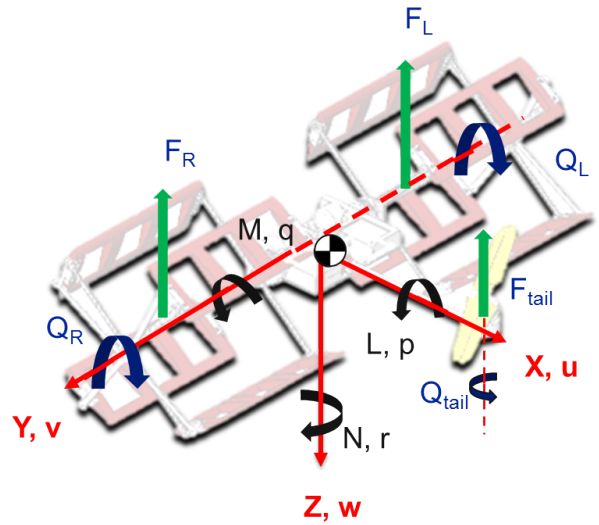


Fig. 18. Forces and moments on the cyclocopter.

in addition to the gyroscopic roll-yaw coupling that is experienced even for the hover case. To gain a better understanding of the effect of collective phasing on the roll-yaw coupling, a flight dynamics model was developed using a first principles approach. The objectives of the simplified linearized model are the following: (1) to qualitatively investigate the effectiveness of the decoupling methodology used in hover when faced with the additional controls coupling encountered in forward flight and (2) to provide a simulation environment in which a preliminary mixing strategy can be developed in conjunction with extensive wind tunnel testing.

FLIGHT DYNAMICS MODEL

For a linearized dynamic model in forward flight, a state space model is considered in the general form:

$$\dot{x} = Ax + Bu \quad (2)$$

The A matrix is composed of the stability derivatives that describe the homogeneous system dynamics and the B matrix contains the control derivatives. The state vectors are $x = [u \ v \ w \ p \ q \ r \ \phi \ \theta]$ and the control inputs are $u = [\delta_{lat} \ \delta_{lon} \ \delta_{throttle} \ \delta_{ped} \ \delta_{phase}]$. δ_{lat} refers to the differential rpm of the two cyclorotors, δ_{lon} is the rpm control of the propeller, δ_{ped} is differential thrust vectoring, and δ_{phase} is the phasing of the cyclic pitch. The most significant simplifications made for the model is that the cyclorotors are governed by rigid-body dynamics and the aerodynamic lift and thrust forces produced by the cyclorotors are obtained in an empirical fashion from the extensive experimental studies on an isolated rotor.

Euler-Newton Equations of Motion

Fig. 18 presents the definition of forces and moments with respect to the body coordinate system. The total applied forces

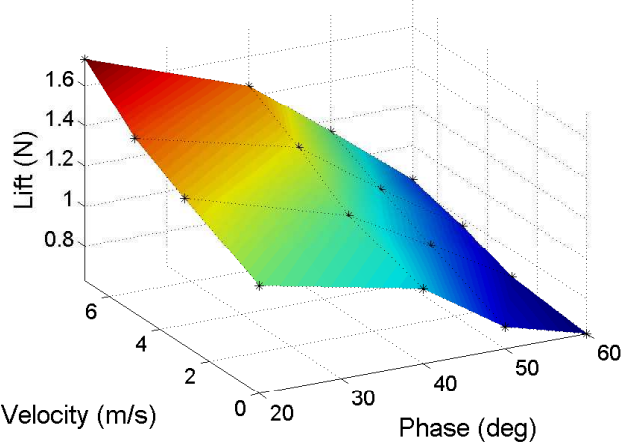


Fig. 19. Variation of lift with velocity and phasing at 1400 RPM.

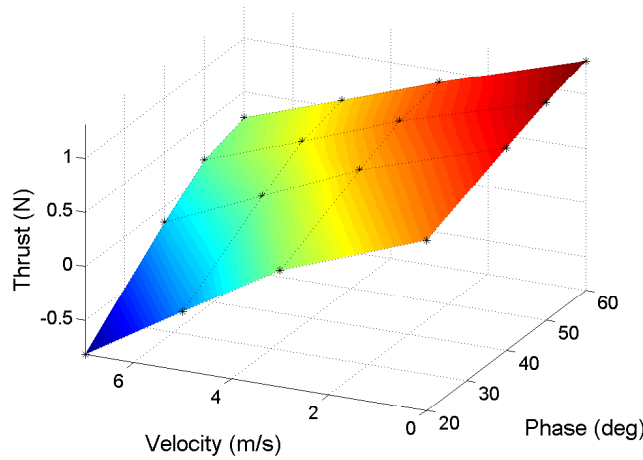


Fig. 20. Variation of thrust with velocity and phasing at 1400 RPM.

and moments can be presented as series of ordinary differential equations as follows:

$$\sum X = m(\dot{u} - rv + qw) + mgsin\theta - F_x + D_x \quad (3)$$

$$\sum Y = m(ru + \dot{v} - pw) - mgsin\phi cos\theta + D_y \quad (4)$$

$$\sum Z = m(-qu + pv - \dot{w}) - mgcos\phi cos\theta + F_z + D_z \quad (5)$$

$$\sum L = I_{xx}\dot{p} - (I_{yy} - I_{zz})qr - F_zd_y + D_yd_z + H_yr \quad (6)$$

$$\sum M = I_{yy}\dot{q} - (I_{zz} - I_{xx})pr - F_zd_x + D_yd_p + D_zd_z - Q_{cyclo} \quad (7)$$

$$\sum N = I_{zz}\dot{r} - (I_{xx} - I_{yy})pq - F_xd_y + D_yd_y - Q_{prop} - H_yp \quad (8)$$

$$\dot{\phi} = p + (qsin\phi + rcos\phi)tan\theta \quad (9)$$

$$\dot{\theta} = qcos\phi - rsin\phi \quad (10)$$

$$\dot{\psi} = (qsin\phi + rcos\phi)sec\theta \quad (11)$$

In these equations, F_x , F_z , and F_p are the lift produced by the cyclorotors and propeller, respectively. The D_x , D_y , and D_z

are drag terms while the d_x , d_y , d_z , and d_p terms are the moment arms. During forward flight, the forces produced by the cyclorotor are influenced by its phase angle, rotational speed, and freestream velocity. These aerodynamic forces are derived through interpolating experimental data. An extensive wind tunnel testing was previously conducted on an isolated cyclorotor in which the effects of airspeed, phase angle, and advance ratios on F_x and F_z were measured (Ref. 8). The results of the study at the constant operational speed of 1400 rpm are plotted showing the variation of F_x and F_z against airspeed and phase angle (Fig. 19, 20). A polynomial curve fit of the surface plot is used to provide a precise representation of rotor forces and moments in forward flight for any given controls input. The coefficients for the drag perturbation forces ($D = k_dV^2$) are also extracted from the same wind tunnel experiments at the appropriate control inputs.

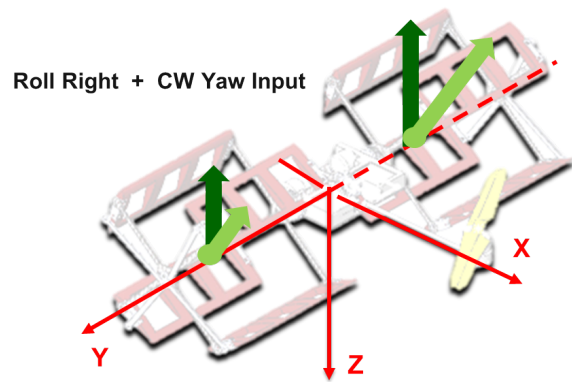
In the equation, the dominant gyroscopic moments produced by the cyclorotors are expressed in terms of angular momentum in the respective axis. The fuselage velocities in body coordinate are $\vec{v}=[u\ v\ w]^T$ and the angular rates are $\vec{\omega}=[p\ q\ r]^T$. The products of inertia terms (I_{xy} , I_{xz} , I_{yz}) have been removed because the cyclocopter is quasi-symmetric about the X-Y and X-Z planes. The vehicle center of gravity was found by weighing individual components that are presented in Table 1. The inertia terms were calculated by setting the components as point masses.

Perturbation Equations

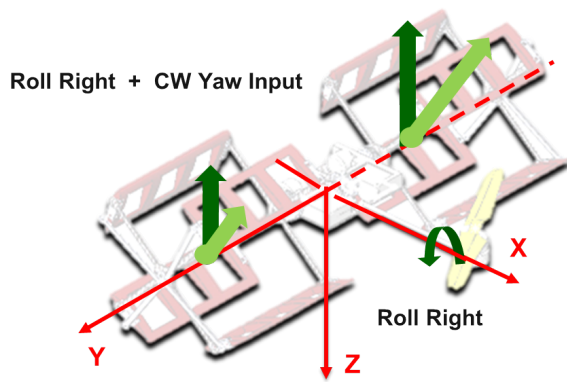
The Euler equations are linearized for small perturbations about a trimmed steady state. The trim condition assumed in level forward flight (v_o , w_o , p_o , q_o , r_o , ϕ_o , θ_o , $\psi_o = 0$) is at a steady 4 m/s forward velocity and 1400 RPM. The appropriate control inputs $u = [\delta_{lat}\ \delta_{lon}\ \delta_{throttle}\ \delta_{ped}\ \delta_{phase}]$ required to balance the forces and moments in trimmed flight is analytically determined and subtracted from the linearized equation to obtain the perturbation equations.

Assuming perturbations are small, the products of the perturbations can be neglected. The perturbation force equations are normalized by vehicle mass and moment equations by the corresponding inertia. The state space model is numerically developed by individually perturbing each state, state derivative, and control to obtain the resultant change in the linearized forces and moments. The resulting nonzero components of the A and B matrices are:

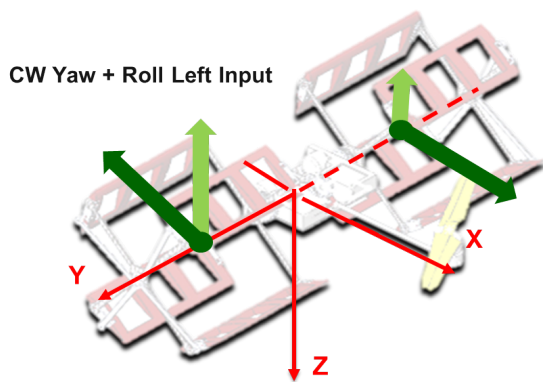
$$A = \begin{vmatrix} X_u & 0 & 0 & 0 & 0 & 0 & 0 & -g \\ 0 & Y_v & 0 & Y_p & 0 & Y_r & g & 0 \\ Z_u & 0 & Z_w & 0 & Z_q & 0 & 0 & 0 \\ 0 & L_v & 0 & L_p & 0 & L_r & 0 & 0 \\ M_u & 0 & 0 & 0 & M_q & 0 & 0 & 0 \\ 0 & N_v & 0 & N_p & 0 & N_r & 0 & 0 \\ 0 & 0 & 0 & 1 & 0 & 0 & 0 & 0 \\ 0 & 0 & 0 & 0 & 1 & 0 & 0 & 0 \end{vmatrix}$$



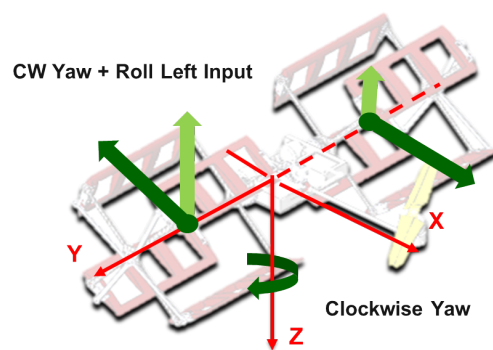
(a) Mixed roll right and clockwise yaw input.



(b) Pure roll right response.



(c) Mixed clockwise yaw and roll left input.



(d) Pure clockwise yaw response.

Fig. 21. Controls mixing for gyroscopic coupling.

$$B = \begin{vmatrix} 0 & 0 & 0 & 0 & X_{phase} \\ 0 & 0 & 0 & 0 & 0 \\ 0 & 0 & Z_{throttle} & 0 & 0 \\ L_{lat} & 0 & 0 & L_{ped} & 0 \\ 0 & M_{lon} & 0 & 0 & 0 \\ N_{lat} & 0 & 0 & L_{ped} & 0 \\ 0 & 0 & 0 & 0 & 0 \\ 0 & 0 & 0 & 0 & 0 \end{vmatrix}$$

Feedback Controls and Mixing

The cyclocopter is highly unstable without attitude stabilization via feedback control system. Therefore, a PD controller is also incorporated into the model. The gains (K) used for the model have been experimentally found in hover using the Ziegler Nichols approach.

$$\dot{x} = (A - BK)x + Bu \quad (12)$$

In order to eliminate gyroscopic coupling (Ref. 6), the roll and yaw controls were appropriately mixed as depicted in Fig. 21. For example, if a roll right response is desired, a roll right input is combined with a clockwise input. Likewise, for a clockwise yaw motion, a clockwise yaw input is appropriately combined with a roll left input.

In forward flight, an additional complication is that the thrust vectors are inclined ($\Phi > 0^\circ$). The mixing discussed above only focuses on the gyroscopic coupling and does not consider effects of phasing or forward velocity.

SIMULATION RESULTS AND DISCUSSION

The purpose of the simulation studies is to determine the effect of phasing on forward flight velocity and to aid in the development of a control strategy to achieve decoupled, steady, level forward flight. An ordinary differential equation solver is used to study the dynamics for the forward flight cases. In the simulation, only simplified models are considered, which allows for development of control strategies in a systematic manner. In addition, by considering only a small number of fundamental parameters, the model provides important insights into the underlying physics involved in forward flight.

Effect of Phasing on Forward Velocity

The first case of simulation is used to determine whether a phasing input is sufficiently able to control forward velocity. The cyclocopter is initially traversing at 4 m/s with phasing of $\Phi = 35^\circ$. Increasing the phasing to $\Phi = 45^\circ$ with a δ_{phase} step input (time = 3 seconds) also causes a step change in velocity (Fig. 22).

It can be observed that at 4 seconds, the airspeed is approaching some equilibrium forward velocity. This is expected as F_x is increasing until it equals D_x . During the acceleration phase, the initial response is large and acceleration begins to decrease with time. When the phase input is returned, the flight speed returns to the original forward velocity at the same rate.

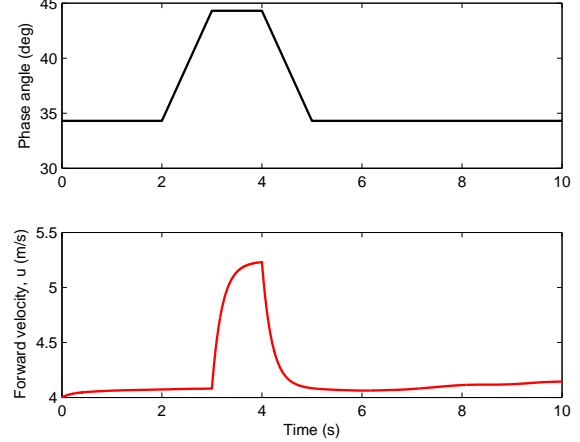


Fig. 22. Forward velocity (u) vs. phase input (Φ).

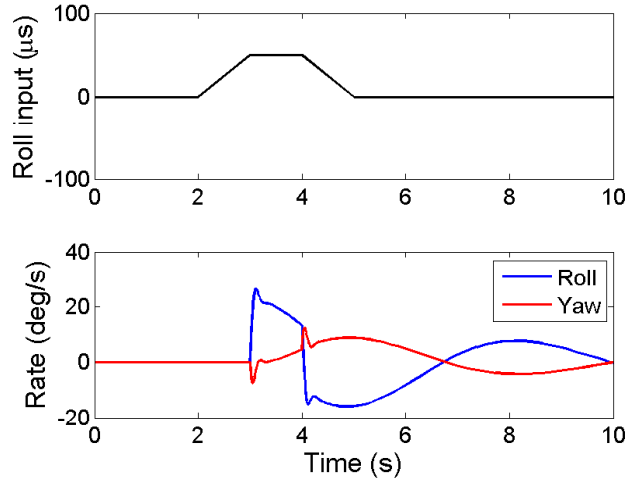


Fig. 23. Attitude rate response for roll left step input at 4 m/s and $\Phi = 35^\circ$.

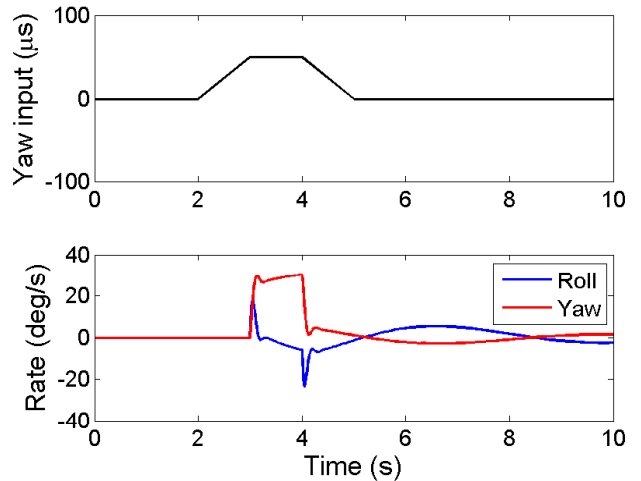


Fig. 24. Attitude rate response for yaw clockwise step input at 4 m/s and $\Phi = 35^\circ$.

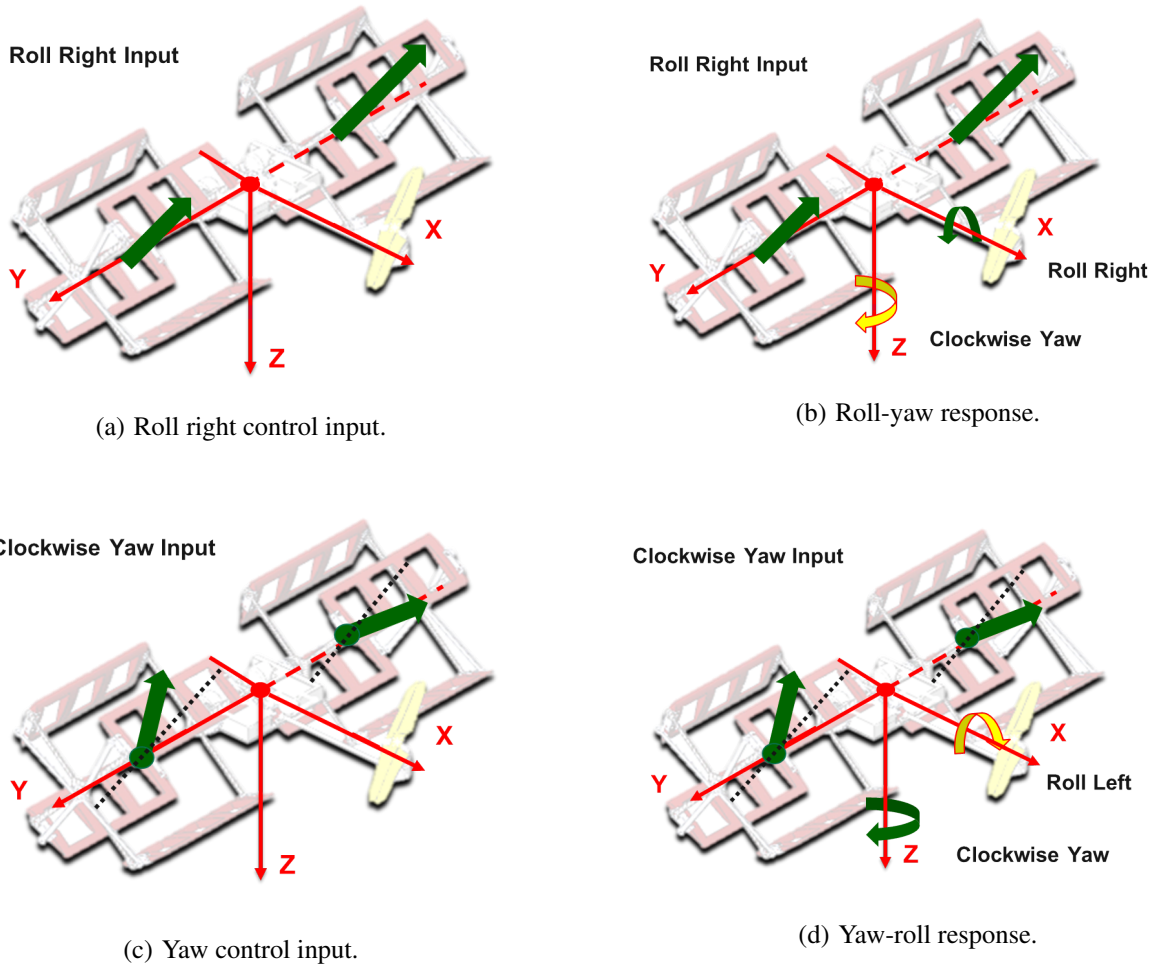


Fig. 25. Controls cross-coupling between roll and yaw degrees of freedom occurring at high phase angles.

Effect of Phasing on Roll-Yaw Coupling

The next case of simulation is to determine whether the gyroscopic mixing found in hover is sufficient to decouple roll and yaw moments in forward flight. For a step roll right input at $\Phi=35^\circ$, there is a corresponding roll right response and a clockwise yaw (Fig. 23). As previously mentioned, for a roll right input, the gyroscopic effect would induce a counterclockwise yaw so an appropriate ratio of clockwise yaw is also provided in hover. However, at $\Phi=35^\circ$, the mixing ratios would need to be reduced in order to decouple the dynamics in forward flight.

Interestingly, a clockwise yaw input induces a roll right response, which is the same type of response caused by gyroscopic coupling (Fig. 24). In this case, the mixing ratios need to be increased in order to adequately decouple the roll and yaw degrees of freedom. The controls coupling at high phase angles is summarized in Fig. 25. The phenomenon can be physically explained by considering the magnitude of F_x and F_z at high phase angles. As the phase angle increases, the thrust vector is tilted towards the +X-axis and thus F_x increases and F_z decreases. A differential change in rotational speed would have a greater effect on yaw than in roll. Likewise, thrust vectoring would effectively cause a roll response.

Based on the simulation results, the modified controls mixing for forward flight is as follows:

$$\delta_\phi = [k_{\phi_{lat}} \delta_{lat} + k_{\phi_{ped}} \delta_{ped}] \sin \Phi \quad (13)$$

$$\delta_\psi = [k_{\psi_{lat}} \delta_{lat} + k_{\psi_{ped}} \delta_{ped}] \sin \Phi \quad (14)$$

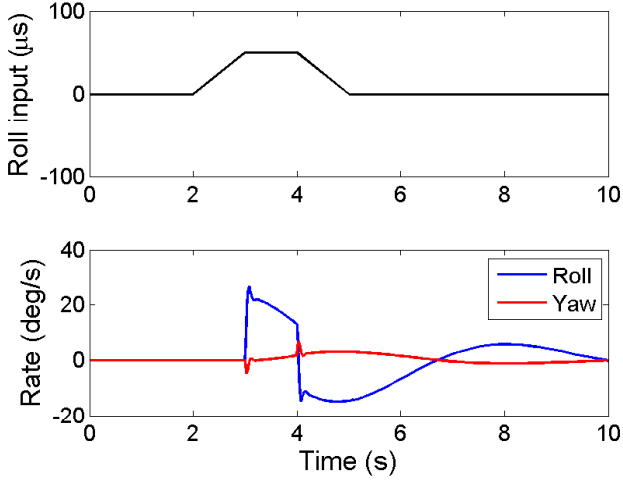


Fig. 26. Attitude rate response for roll left step input at 4 m/s and $\Phi = 35^\circ$ with controls mixing.

The above terms are added to the original mixing used in hover to eliminate gyroscopic couplings. The coefficients of the control inputs are the mixing ratios in forward flight. After incorporating the mixing in the model, step roll and yaw inputs are again simulated. Figs. 26 and 27 show that this form of controls mixing can be used to decouple the roll and

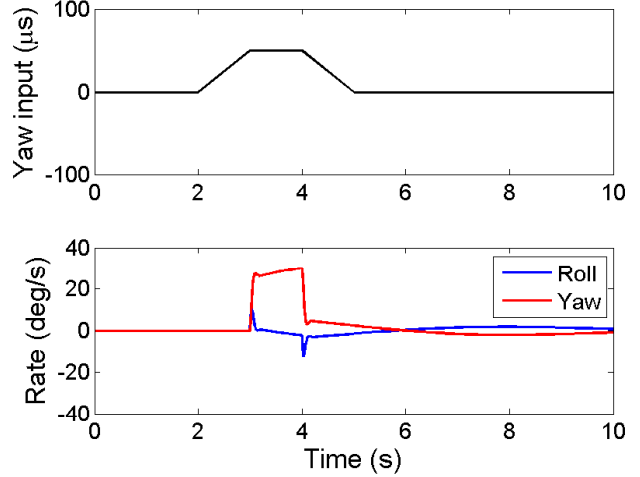


Fig. 27. Attitude rate response for yaw clockwise step input at 4 m/s and $\Phi = 35^\circ$ with controls mixing.

yaw degrees of freedom in forward flight. Overall, the model is used to determine baseline coefficient values and assisted in setting the wind tunnel testing methodology. These coefficients were further refined in the wind tunnel and explained in the next section.

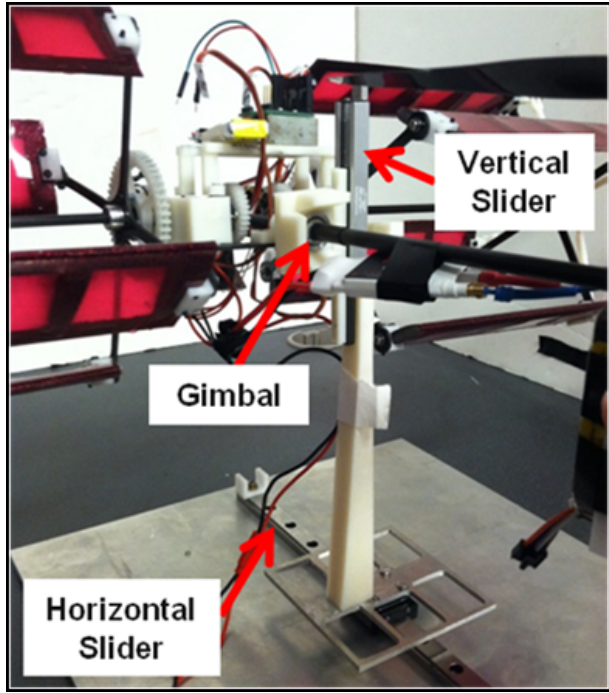
WIND TUNNEL EXPERIMENT

Compared to the model, the wind tunnel experiments provide a more realistic vehicle response to variation of phasing and airspeed in forward flight. The objectives of the wind tunnel testing of the cyclocopter are as follows: (1) understand the effect of forward velocity and phase angle on vehicle dynamics, (2) systematically find the appropriate mixing ratios required to decouple the roll-yaw couplings at various operating forward velocities, and (3) quantify the control inputs required to maintain a trimmed level forward flight (total F_z = weight, $F_x = D_x$).

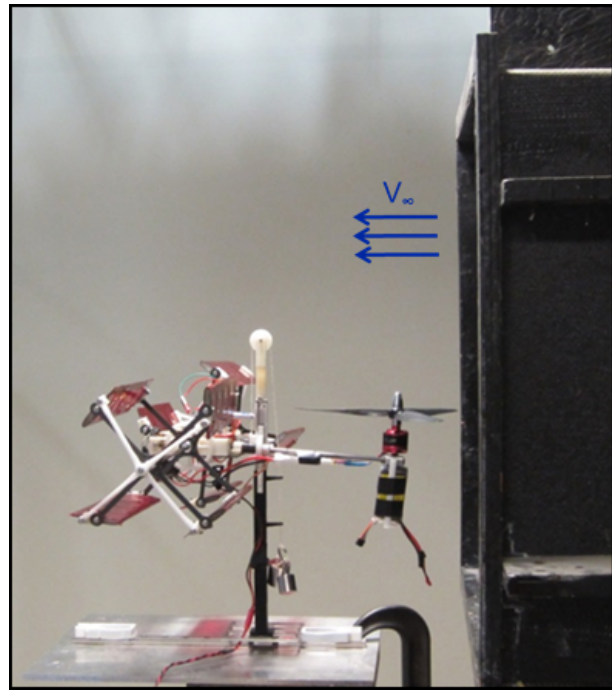
One of the challenges of accurately simulating forward flight conditions in the wind tunnel was to develop an experimental setup that would enable 5-DOF motions without significantly introducing additional damping into the system. The vehicle was mounted on a spherical gimbal at CG, which allowed free rotation in pitch, roll, and yaw (Fig. 28(a)). The entire setup was then augmented with a horizontal and a vertical slider to enable forward translation and heave. Only the lateral translation was restricted due to the physical constraints set by the wind tunnel.

The open-jet wind tunnel consists of a square test section dimensions of 0.56 meters (22 inches) in length and width (Fig. 28(b)). The vehicle was restricted to maximum horizontal translation from reference trim location (center of slider) of ± 0.178 meters (7 inches) and a positive heave of 0.051 meters (2 inches). Rotations about pitch, roll, and yaw were mechanically restricted to $\pm 45^\circ$.

The control inputs in this experimental study were airspeed (V_∞), phase angle (Φ), and rotational speed (Ω). A systematic

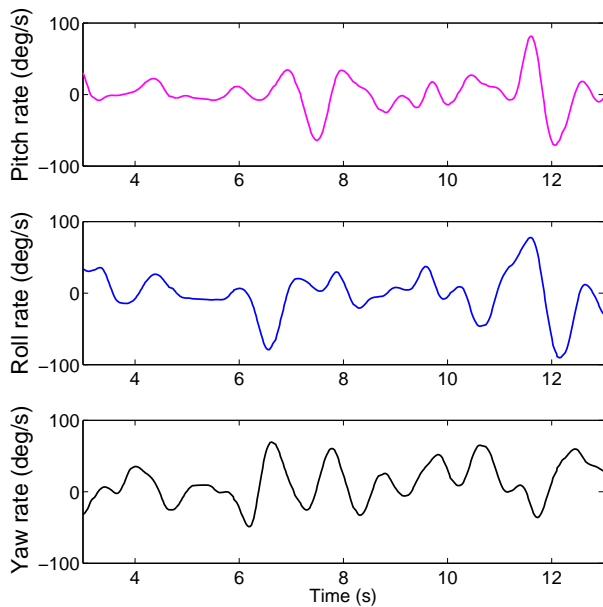


(a) 5-DOF experimental stand for wind tunnel testing.

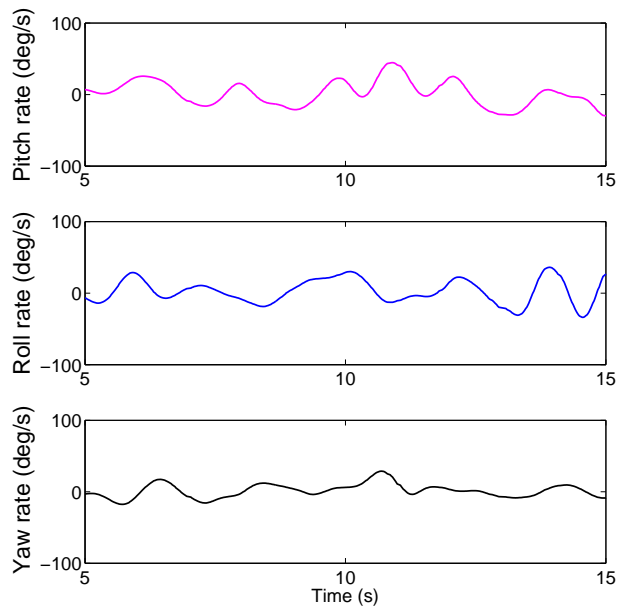


(b) Wind tunnel testing setup.

Fig. 28. Wind tunnel testing setup.

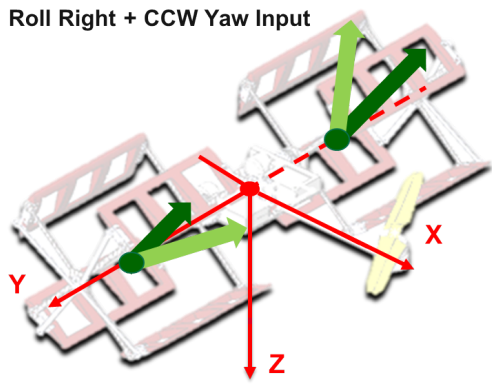


(a) Presence of strong roll-yaw coupling.

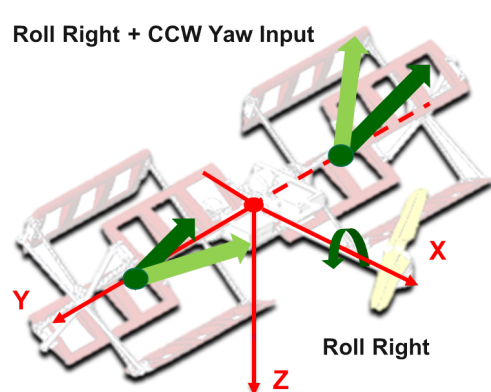


(b) After implementing controls mixing.

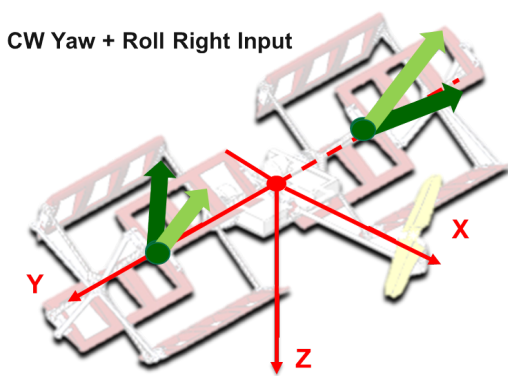
Fig. 29. Attitude rates at 4 m/s and 45 deg phasing.



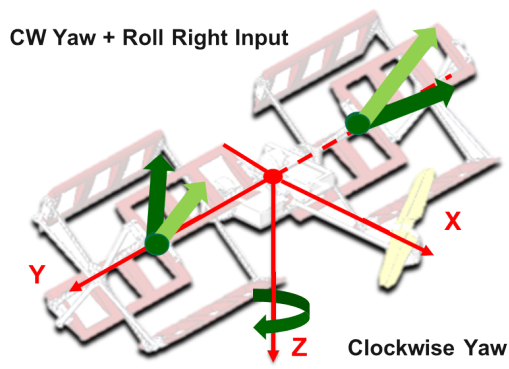
(a) Mixed roll right and counterclockwise yaw input.



(b) Pure roll right response.



(c) Mixed clockwise yaw and roll right input.



(d) Pure clockwise yaw response.

Fig. 30. Controls mixing for forward flight.

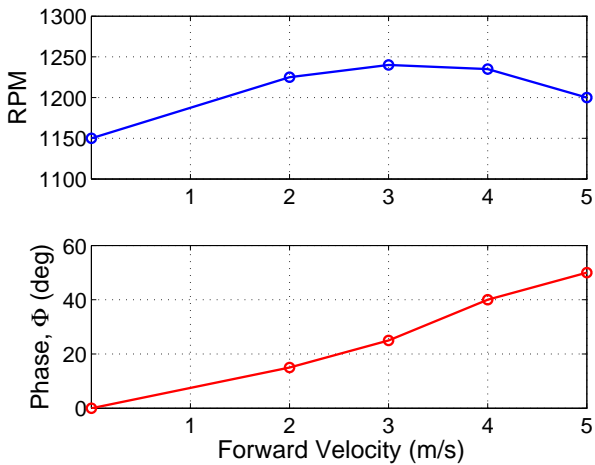


Fig. 31. Controls inputs required to obtain trimmed free flight (lift = weight, thrust = drag).

velocity sweep from 2 to 5 m/s was conducted at intervals of 1 m/s. At each velocity, the phase angles were varied from 0° to 50° in increments of 5° . The rotational speed was varied such that the cyclocopter always maintained a positive displacement on the vertical slider. This represents the trim condition where lift is equivalent to total vehicle weight. Throttle (collective cyclorotor rpm), pitch (propeller rpm), roll (differential cyclorotor rpm), yaw (differential phasing), and forward velocity (collective phasing) inputs were given so that the vehicle maintained its reference trim position on the horizontal slider without pitch, roll, or yaw moments.

Effect of Phasing and Forward Velocity on Coupling

To understand the effect of phasing on the roll-yaw coupling, the rotational speed and airspeed are kept constant as phasing increases. Throughout the process, the feedback control system is trying to stabilize the vehicle attitude. In one case, the cyclorotor rotational speed is kept at a constant 1200 RPM and the airspeed is maintained at 2 m/s. Starting from $\Phi=0^\circ$, the phasing is incrementally increased by $\Phi=5^\circ$. As the phasing approaches $\Phi=15^\circ$, there is an observable oscillation in the roll and yaw degrees of freedom.

As predicted by the linearized cyclocopter model, increasing the phasing results in a noticeable increase in roll-yaw coupling when at a constant forward velocity. As previously mentioned, the coupling is due to the increase in magnitude of the propulsive forces at high phase angles. Therefore, thrust vectoring has a larger impact on the roll moments and subsequently, changes in rotor RPM have a greater influence on yaw moments. In addition, the mixing ratios found in the wind tunnel were similar to the ratios estimated from the simple model.

A significant finding from the experiment is that for a constant phasing, varying forward velocity does not significantly impact the coupling beyond the capabilities of the flight controller that was implemented. While forward velocity affects the lift produced by the cyclocopter, the feedback control system is able to stabilize any imbalance in the longitudinal dy-



Fig. 32. First successful forward flight of a twin-cyclocopter ($V = 3$ m/s).

namics. Since the roll-yaw coupling is only dependent on phase, mixing ratios of roll and yaw inputs only vary with phase and not forward velocity. Fig. 29 displays the attitude rates of the cyclocopter at 4 m/s and $\Phi = 45^\circ$ before and after implementing the mixing ratios. It is evident that using the mixing ratios, there is a significant reduction in roll-yaw coupling along with improved vehicle stability.

The finalized forward flight control strategy is depicted in (Fig. 30). A positive roll (right) input results in an increase in rpm of the left rotor and a decrease in the right rotor. At higher phases, this leads to positive yaw (clockwise). If the positive roll input is accompanied by a negative yaw (counterclockwise), it would negate the effects of the rpm on yaw and result in a pure roll output. Likewise, a positive yaw input would be paired with a negative roll input to accomplish a pure yaw output.

Control Inputs for Trimmed Forward Flight

A sweep of forward velocities and phasing was conducted to find the appropriate control inputs needed to achieve steady level flight (thrust = drag, lift = weight) at each velocities. At a constant forward velocity and phasing, increasing the rotational speed results in an increase of both lift and thrust and consequently, an increase in power. Increasing phasing of the cyclorotors, while keeping both the forward velocity and

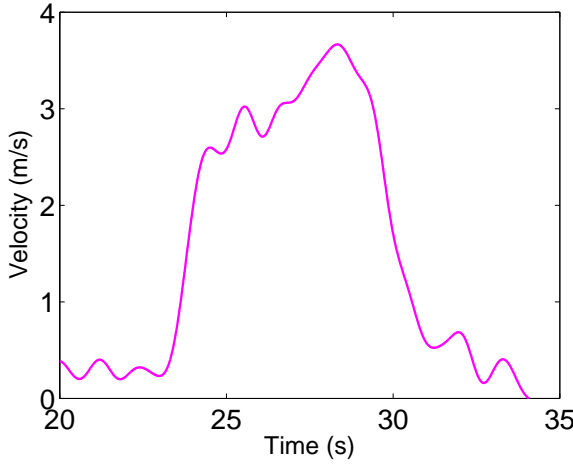


Fig. 33. Airspeed data taken shows forward velocity of 3.5 m/s.

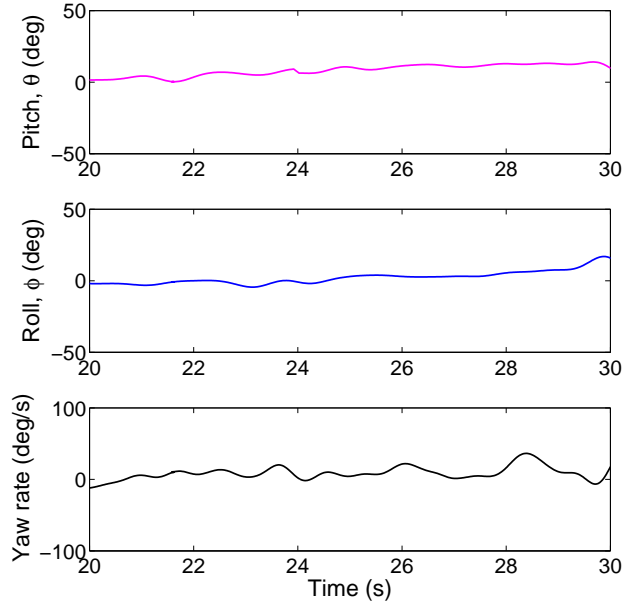


Fig. 35. Cyclocopter attitude in steady level forward flight.
FLIGHT TEST RESULTS

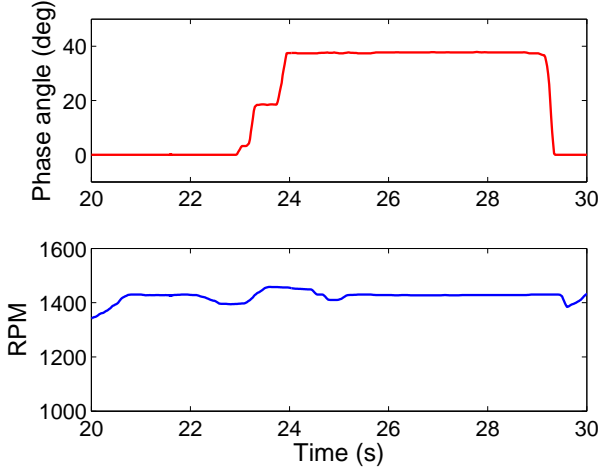


Fig. 34. Phase angle ($\Phi = 35^\circ$) and rotational speed (1400 RPM) during forward flight at 3.5 m/s.

rpm constant, results in an increase in thrust and a decrease in lift. Therefore, to increase steady level flight speed from a trimmed condition, both the phasing and rpm is simultaneously adjusted.

As the forward velocity increases, the required phasing increases almost linearly while the required rpm decreases (Fig. 31). Limitations on the current maximum achievable forward flight are caused by significant vehicle drag since the fuselage of the cyclocopter is not aerodynamically clean. Theoretically, the maximum forward velocity is achieved at $\Phi = 90^\circ$. For future studies, the fuselage of the cyclocopter will be aerodynamically cleaner and further efforts will be made to reduce parasitic drag. Overall, the insights gained from the wind tunnel experiments show that the forward flight control strategy and feedback control system is suitable for free flight testing.

During the flight tests, the proportional and derivative gains were tuned using the Ziegler Nichols approach. The gains that offered acceptable stiffness and damping to reject external disturbance with minimal oscillations were chosen. While the form of the control strategy is fixed, the gains and control inputs for trimmed flight varied slightly from the ones obtained through wind tunnel testing because the cyclocopter was previously constrained in a gimbal setup that provided additional damping in pitch, roll, and yaw. Additional variation was caused by shifts in the moments of inertia because the cyclocopter is equipped with a single 3S 11.1 volt 850 mAh Lithium-Polymer battery weighing 75 grams and attached directly under the propeller motor.

Flight tests were systematically conducted by first providing a pure throttle command and observing the vehicle response. Any forward translation was counteracted by either reducing the phasing of the cyclic blade pitch or varying the propeller rpm. After trimming the cyclocopter, level forward flight is then initiated solely through thrust vectoring of the cyclorotors.

The present vehicle has successfully demonstrated steady level forward flight up to a maximum of 5 m/s forward velocity (Fig. 32). As seen from Figs. 33, 34, and 35, a satisfactory steady level forward flight is obtained with the pitch and roll angles held close to zero and minimum offsets in yaw rate. The flight data shown is at 3.5 m/s and $\Phi = 35^\circ$ with the rotational speed maintained at 1400 rpm.

At these control settings, roll and yaw inputs were given to demonstrate decoupled roll-yaw moments. Fig. 36 shows the vehicle response for a negative roll input (roll left) plotted against the attitude rates and roll Euler angle. The roll step input is given at time = 9 seconds. An immediate perturbation in the roll rate is observed without significant changes

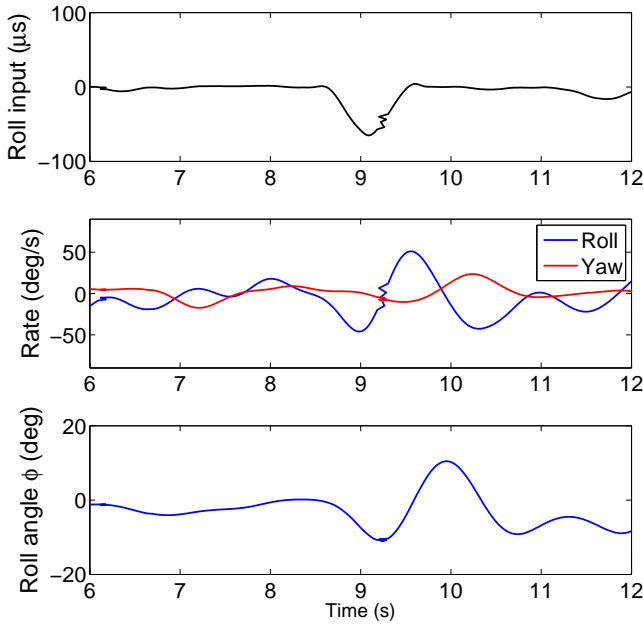


Fig. 36. Roll left pilot input ($t = 9\text{s}$) results in pure roll response.

in the yaw rate. Interestingly, the feedback overshoots when trying to stabilize the roll moment, but quickly manages to recover the trim state. This suggests that gains need to be further fine tuned. It is challenging to tune the gains in forward flight without potentially crashing the vehicle, so the gains were tuned in hover. Similar trends are observed for a counter-clockwise yaw input as seen in Fig. 37.

The mixing ratios found in the wind tunnel were again fine tuned during free flight tests. There was a notable difference in the ratios, which can be attributed to the additional damping provided by the test stand and changes in vehicle inertia when mounting batteries. While the ratios found in the wind tunnel were similar for both roll-yaw and yaw-roll couplings, the ratios for yaw-roll coupling is much greater in flight. The vehicle is observed to be much more susceptible to yaw-roll coupling at high phase angles. This is due to the fact that both the gyroscopic coupling and the controls coupling induce a similar response for a yaw input and opposite responses in roll (Fig. 17, 25).

The 550 gram twin-cyclocopter is currently the first forward flight capable cyclocopter in literature that has successfully utilized thrust vectoring to gain forward velocity instead of pitching the vehicle forward. Thrust vectoring has distinct advantages that can be used to radically improve performance and expand the flight envelope of the future cyclocopters.

CONCLUSIONS

The objective of this research was to expand the cyclocopter flight envelope to stable, high-speed level forward flight. The present work focused on developing a forward flight control strategy for the twin-cyclocopter using a combination of independent pitch phasing and rotational speed control of the two

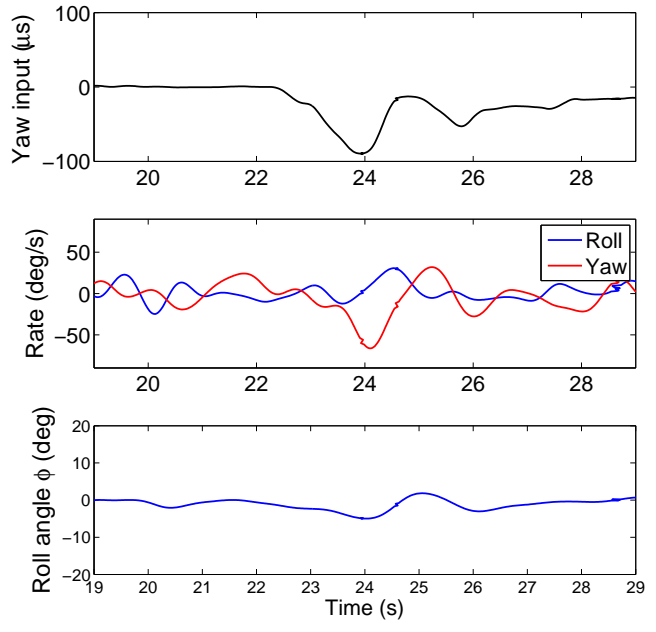


Fig. 37. Yaw clockwise pilot input ($t = 24\text{s}$) results in pure yaw rate response.

cyclorotors, along with the tail rotor, without relying on any additional control by means of a traditional empennage system. While the strategy facilitates efficient, high-speed steady level forward flight, it is accompanied by a strong yaw-roll control cross-couplings. These are in addition to the gyroscopic couplings that are experienced even in hover. To understand the presence of coupling in forward flight and to evaluate the effectiveness of decoupling methods, a flight dynamics model of forward flight was developed using a first principles approach. The model demonstrated that these couplings are the result of tilting the thrust vector during forward flight. The wind tunnel studies showed that the mixing ratio was a function of phasing of blade cyclic pitch, especially at high phase angles. Therefore, a control mixing algorithm was implemented that actively changed during flight with phase angle. The current flight tests resulted in steady level forward flight up to 5 m/s. The following is the summary and some of the specific conclusions drawn from this study:

1. The cyclocopter is inherently unstable and requires an inner-loop attitude stabilization. A proportional-derivative controller for the feedback controls system can sufficiently stabilize the vehicle. ELKA, an ultra-light (1.3 grams) onboard processor-sensor board was successfully developed for the cyclocopter and is able to update the inner-loop attitude stabilization at 500 Hz.
2. Phasing of the cyclic pitch provides enough change in propulsive force to increase forward velocity of the vehicle and enables level forward translation. The rate of transition from hover to forward flight depends entirely on the phasing input. When transitioning back to hover, the cyclocopter is able to abruptly come to an immediate

stop even while moving at reasonable forward velocities. Therefore, the tilting of the cyclorotor thrust vector provides complete control authority of the forward velocity. The pilot controls in forward flight include throttle (collective cyclorotor rpm), pitch (propeller rpm), roll (differential cyclorotor rpm), yaw (differential phasing), and forward velocity (collective phasing).

3. A strong existence of gyroscopic and control cross couplings were observed in forward flight. These were studied using a first principles based flight dynamics model. Simulation results demonstrated that additional coupling in forward flight is present at high phase angle. The coupling is due to the increase of magnitude of propulsive forces at high phase angles. As a result, thrust vectoring has a larger impact on the roll moments and subsequently, changes in rotor RPM have a greater influence on yaw moments.
4. The wind tunnel experiments showed that for a constant phasing, varying forward velocity does not impact the coupling. While forward velocity affects the lift produced by the cyclocopter, the feedback control system is able to stabilize any imbalance in the longitudinal dynamics.
5. Decoupling the roll and yaw degrees of freedom in forward flight involves mixing pilot roll and yaw inputs. If a positive roll input is accompanied by a negative yaw (counterclockwise), it would negate the effects of the rpm on yaw and result in a pure roll output. Likewise, a positive yaw input would be paired with a positive roll input to accomplish a pure yaw output. The gyroscopic coupling and controls coupling induces the same positive roll response for a positive yaw input and differ for a roll input.
6. The 550 gram twin-cyclocopter is currently the first forward flight capable cyclocopter in literature that has successfully utilized thrust vectoring to gain forward velocity instead of pitching the vehicle forward. The present vehicle has successfully demonstrated steady level forward flight up to a maximum of 5 m/s forward velocity.

ACKNOWLEDGEMENT

This research was supported by the Army's MAST CTA Center for Microsystem Mechanics with Dr. Brett Piekarski (ARL) and Mr. Chris Kroninger (ARL-VTD) as Technical Monitors.

REFERENCES

¹Pines, D., and Bohorquez, F., "Challenges Facing Future Micro-Air-Vehicle Development," *Journal of Aircraft*, Vol. 43, (2), March/April 2006, pp. 290–305.

²Leishman, J.G., *Principles of Helicopter Aerodynamics* (Cambridge Univ. Press, New York, 2000).

³Benedict, M., Shrestha, E., Hrishikeshavan, V., and Chopra, I., Development of 200 gram Twin-Rotor Micro Cyclocopter Capable of Autonomous Hover, Proceedings of the American Helicopter Society Future Vertical Lift Aircraft Design Conference, San Francisco, CA, January 18-20, 2012.

⁴Shrestha, E., Benedict, M., Hrishikeshavan, V., and Chopra, I., Development of a 100 gram Micro Cyclocopter Capable of Autonomous Hover, Proceedings of the 38th European Rotorcraft Forum, Amsterdam, Netherlands, September 47, 2012.

⁵Benedict, M., Gupta, R., and Chopra, I., Design, Development and Flight Testing of a Twin-Rotor Cyclocopter Micro Air Vehicle, Proceedings of the 67th Annual National Forum of the American Helicopter Society, Virginia Beach, VA, May 35, 2011.

⁶Hrishikeshavan, V., Benedict, M., and Chopra, I., Flight Dynamics Identification of a Cyclocopter Micro Air Vehicle in Hover, Proceedings of the 69th Annual National Forum of the American Helicopter Society, Phoenix, Arizona, May 21-23, 2012.

⁷Benedict, M., Jarugumilli, T., Lakshminarayan, V., K., and Chopra, I., Experimental and Computational Studies to Understand the Role of Flow Curvature Effects on the Aerodynamic Performance of a MAV-Scale Cycloidal Rotor in Forward Flight, Proceedings of the 53rd AIAA/ASME/ASCE/AHS/ASC Structures, Structural Dynamics, and Materials Conference, Honolulu, Hawaii, April 23-26, 2012.

⁸Jarugumilli, T., Benedict, M., and Chopra, I., Experimental Investigation of the Forward Flight Performance of a MAV-Scale Cycloidal Rotor, Proceedings of the 68th Annual National Forum of the American Helicopter Society, Fort Worth, TX, May 13, 2012

⁹Benedict, M., Jarugumilli, T., and Chopra, I., "Experimental Investigation of the Effect of Rotor Geometry on the Performance of a MAV-Scale Cycloidal Rotor," Proceeding of the International Specialists' Meeting on Unmanned Rotorcraft, Tempe, AZ, January 25–27, 2011.

¹⁰Benedict, M., "Fundamental Understanding of the Cycloidal-Rotor Concept for Micro Air Vehicle Applications," Ph.D Thesis, Department of Aerospace Engineering, University of Maryland College Park, December 2010.

¹¹Benedict, M., Jarugumilli, T., and Chopra, I., "Experimental Performance Optimization of a MAV-Scale Cycloidal Rotor," Proceedings of the AHS Specialists' Meeting on Aeromechanics, San Francisco, CA, Jan 20–22, 2010.

¹²Benedict, M., Shrestha E., Hrishikeshavan, V., and Chopra, I., "Development of a 200 gram Twin-Rotor Micro Cyclocopter Capable of Autonomous Hover," American Helicopter Society Future Vertical Lift Aircraft Design Conference, San Francisco, CA, January 18-20, 2012.

¹³Benedict, M., Mattaboni, M., Chopra, I., and Masarati, P., "Aeroelastic Analysis of a MAV-Scale Cycloidal Rotor," Proceedings of the 51st AIAA/ASME/ASCE/AHS/ASC Structures, Structural Dynamics, and Materials Conference, Orlando, FL, April 12–15, 2010.

¹⁴Benedict, M., Ramasamy, M., Chopra, I., and Leishman, J. G., "Performance of a Cycloidal Rotor Concept for Micro Air Vehicle Applications," *Journal of American Helicopter Society*, Vol. 55, No. 2, April 2010, pp. 022002-1 - 022002-14.

¹⁵Yeo, D., Atkins, E., Bernal, L. and Shyy, W., Aerodynamic Sensing for a Fixed Wing UAS Operating at High Angles of Attack, AIAA 2012-4416 Proc. AIAA Atmospheric Flight Mechanics Conference, 13-16 August 2012, Minneapolis Minnesota.

¹⁶Georgy, J., Noureldin, A., Korenberg, M., and Bayoumi, M., "Modeling the Stochastic Drift of a MEMS-Based Gyroscope in Gyro/Odometer/GPS Integrated Navigation," IEEE Transactions on Intelligent Transportation Systems, Vol. 11, (4), Dec 2010, pp. 856–872.

¹⁷Y. K. Thong, M. S. Woolfson, J. A. Crowe, B. R. Hayes-Gill, and R. E. Challis, "Dependence of inertial measurements of distance on accelerometer noise", Meas. Sci. Technol., Vol. 13 , (8), pp.1163–1172 , 2002.